Available online www.worldscientificnews.com

World Scientific News

An International Scientific Journal

WSN 219 (2026) 170-195 EISSN 2392-2192

Modeling of Power Generation in a Smart Grid-Connected Hybrid Solar-Wind Energy Conversion System with an Incorporated Ultracapacitor

Gbeminiyi M. Sobamowo[1], Alozie N. Sabinius[2], Adesina A. Oluwole[3], Emmanuel T. Elijah[4], Olalekan J. Lawal[5], Olagbemiro B. Simon[6], Aiyedun O. Emmanuel[7], Olugbemi O. Joshua[8]

[1,2,3,4,5,6,7] Department of Mechanical Engineering, Faculty of Engineering, University of Lagos, Nigeria

[3] Department of Mechanical Engineering, Faculty of Engineering, Yaba College of Technology, Nigeria

[8] Department of Mechanical Engineering, Faculty of Engineering, Lagos State University, Epe Campus, Epe, Lagos, Nigeria

https://doi.org/10.65770/IAHL7422

ABSTRACT

The non-controllable variability, partial unpredictability, and location dependence of a hybrid solar-wind energy conversion system require the incorporation of additional energy system balance supply and demand on grid-on instantaneous basis. However, increased penetration of renewable generation on the power grid imposes serious challenges for generation owners and grid operators. A fully integrated and intelligent distribution energy management system will obviate these challenges. Indisputably, implementation of smart grid system will enable the integration in a reliable manner. Also, the hybrid system is required to be optimized such that reasonable generation schedules are generated in order to satisfy the consumer needs in terms of energy quality and microgrid reliability. In order to achieve this, the power generation in the system has to be modeled. Therefore, this work focuses on modeling of power generation in a smart grid-connected hybrid solar-wind energy conversion system with an incorporated ultracapacitor. Mathematical models are developed for various components of the system. Also, the models are simulated, and the effects of various parameters on the power generation and energy quality of the intelligent hybrid system are investigated. It is therefore hoped that the present study will assist in the optimization of the system for power generation.

Keywords: Mathematical models, Power Generation, Smart grid, Hybrid Solar-Wind, Energy Conversion System, Ultracapacitor.

(Received 7 July 2026; Accepted 21 August 2026; Date of Publication 28 September 2026)

1. INTRODUCTION

The explosive increase in the world population and the exponential rise in world energy demand dwindle the sources of fossil fuels and increase pollution levels in the environment. The undeniable evidences of the limitations, the forecasts of further detrimental trends, non-renewability nature of the high-grade energy source in meeting the present and future world energy demands have been the driving forces behind meeting world energy demands through renewable energy sources. Among the renewable power sources, solar and wind have experienced a rapid growth in the past 25 years. The complementary behavior of wind and solar power sources can be used to design a reliable hybrid power system by combining these two renewable energy sources. However, the drawback in wind and solar energy sources is their unpredictable characteristics, which limits their implementations as the primary energy sources in rural areas. Also, the non-linearity and complexity of the hybrid power systems (HPS) make power management of HPS challenging. Solar and wind powers, being heavily fluctuating, exhibit highly stochastic patterns. Therefore, a variety of problems, such as management of power delivered to the load, arise when such a hybrid system is integrated with the grid or to the load. This challenge can be mitigated by combining other energy sources to the hybrid system. In general, hybrid power system converts all these resources into one form (typically electrical), stores the energy, and the aggregated output is used to supply various loads. The integration of hybrid energy sources with energy storage devices as depicted in Fg. 1 has introduced the concept of microgrid. Such microgrid installations power hybrid solar and wind systems is identified as a strong contender to address current energy needs in rural electrification projects in remote parts of the world. One of the key factors in ensuring smart electric power with effective and sustainable operation of rural microgrid projects is smart energy management approach. The smart microgrid energy management system is responsible for ensuring coordinated energy production and consumption patterns. It uses computational thinking principles to process historical energy consumption patterns with forecasted supply patterns in order to determine the optimal microgrid next-day operational scheduling policy. The determined regulation schedule is subsequently communicated to the real time microgrid controller, which is tasked with the actual coordinated microgrid operation over the course of the following day. By employing appropriate data collection systems such as smart meters and applying appropriate machine learning techniques, it is possible to develop effective microgrid operational schedules to improve system performance and enhance the project sustainability. However, energy management system such as shown in Fig. 1 within the proposed hybrid solar and wind microgrid needs to be optimized such that reasonable generation schedules are provided in order to satisfy the consumer needs in terms of energy quality, microgrid reliability, and family budget. In order to optimize the hybrid system, the power generation chain of the system must be adequately modeled and controlled. Also, dynamic modeling of various components of this system are required to be analyzed. Consequently, Chen et al. [1] developed a detailed dynamic model and simulation of a solar cell/wind turbine/fuel cell/ultracapacitor hybrid power system, while El-Tamaly and Mohammed [2] uses Matlab/Simulink to develop a PV/Wind hybrid electric power system interface with electric utility. In another work, de Souza et al. [3] proposed a hybrid system of the pilot project which composed of 21 kW solar PV power, 22.5 kW rated wind power, 120 batteries of 150 Ah each, and a 53 kVA/48 kW diesel generator as a backup unit in Lençóis Island, located in the north area of Brazil. In order to satisfy the changeable load power demand and to maintain the state of charge of the battery bank to prevent blackout and to extend the life of the batteries, an overall control strategy for power management among different energy sources in a multisource energy system is needed. To this end, Valenciaga and Puleston [4] presented a comprehensive supervisor control for a hybrid system that comprises wind and photovoltaic generation subsystems, a battery bank, and an ac load is developed.

Wang and Nehrir [5] proposed an overall control strategy for a hybrid renewable energy system, in which the wind generation system is controlled by a pitch angle controller and a PV electricity generation unit is controlled by a maximum power point tracking (MPPT) controller. Li et al. [6] introduced the hardware realization of the energy management and control subsystem of a gridconnected wind/solar Hybrid power system. An important issue in hybrid renewable systems is to optimally size the hybrid system components with possible minimum investment and operating costs. Yang [7] recommended an optimal design model for hybrid solar–wind system. The system employs battery banks to calculate the system's optimum configurations in China. Dihrab [8] presented a hybrid solar-wind system as a renewable source of power generation for grid connected application in three cities in Iraq. Reichling [9] modeled a hybrid solar wind power plant in south western Minnesota for a two-year period, using hourly solar irradiation and wind speed data. Ekren [10] showed an optimum sizing procedure of PV/wind hybrid system in Turkey, while Kim [11] developed a grid-connected photovoltaic model using PSCAD/EMTDC for electromagnetic transient analysis. Chayawatto [12] developed a mathematical model of a DC/AC full-bridge switching converter with current control for PV gridconnected system under islanding phenomena. Onar [13] modeled a hybrid wind/FC/ ultra-capacitor (UC) power system for a grid-independent user with appropriate power flow controllers. Villalva et al. [14] presented a comprehensive approach to modeling and simulation of photovoltaic arrays. De Battista et al. [15] investigated power conditioning for a wind-hydrogen energy system. Tsai [16] implemented an insulation-oriented PV model using MATLAB/SIMULINK software package. Said et al. [17] presented different sizing techniques and optimization techniques for off-grid PV–Wind hybrid systems. El-Tamaly et al. [18] designed and optimized (multi-objective optimization) the size of hybrid energy systems under smart grid theories that divide the load into high and low priorities while Shi et al. [19] applied the preference-inspired coevolutionary algorithm to the design of multi-objective hybrid renewable energy system. Ismail et al. [20] modeled an optimal design of a PV/battery/micro-turbine hybrid energy system to supply power to remote communities by using genetic algorithm. Hosseinalizadeh et al. [21] designed techno-economically optimized systems by simulating behavior of various combinations of renewable energy systems with different sizing, including wind turbine (WT), photovoltaic (PV), fuel cell (FC), and battery banks. The above reviewed works are not based on the holistic and effective modeling of the power generation chain through each component of the hybrid system. Therefore, this paper focuses on modeling the power generation in a smart grid-connected hybrid solar-wind energy conversion system with an incorporated ultracapacitor.

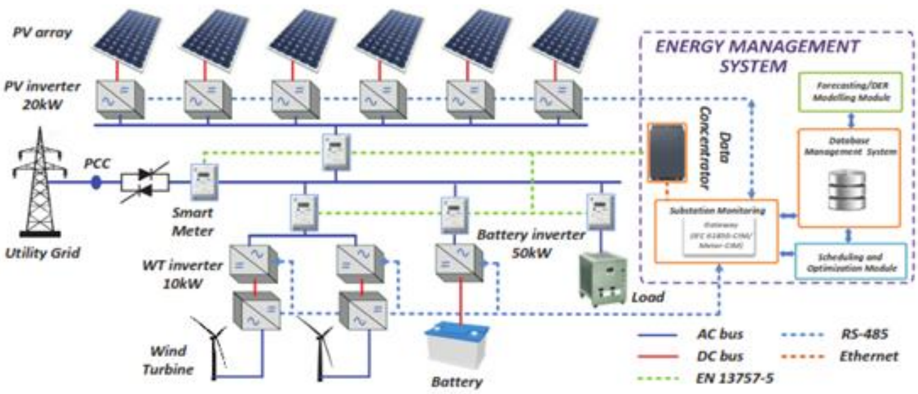

Figure 1. Schematic Diagram of a Multi-Solar Panel-Dual Wind Turbine Hybrid Solar-Wind Energy System.

2. MODEL DEVELOPMENT OF THE POWER GENERATION SYSTEM

Development of power generation by the hybrid system is carried out based on component by component modeling. Consider the solar-wind hybrid system shown in Fig. 2 below, our first attempt in this work is to model the power generation by considering different power sections of the system.

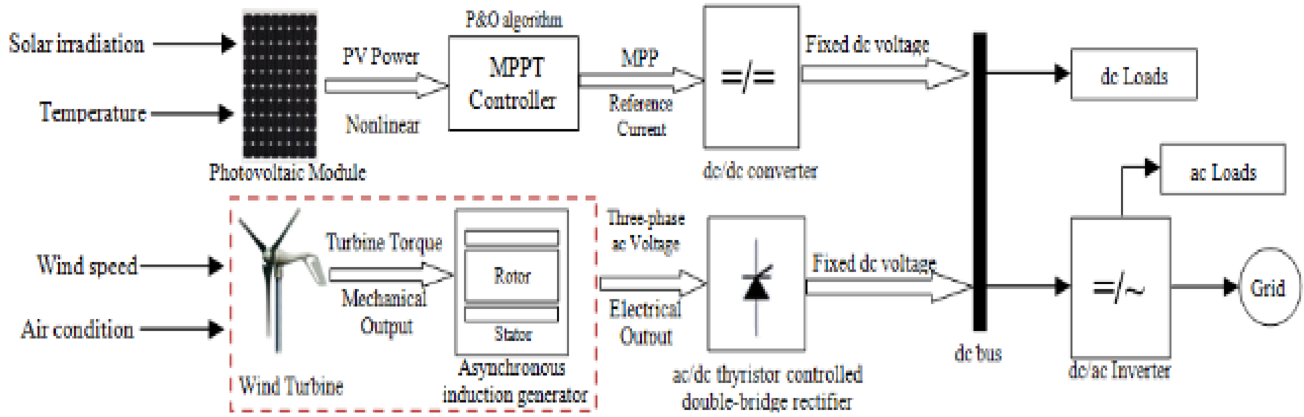

Figure 2. Schematic Diagram of a Single Solar Panel-Single Wind Turbine Hybrid Solar-Wind Micro-Grid System [22].

2.1. Modeling the Electrical Characteristics of Photovoltaic Cell (Solar Cell)

The performance of photovoltaic modules is high dependent on both the availability of solar radiation in the locality and the temperature of photovoltaic cells. The analysis and the knowledge of photovoltaic modules are important in the design of photovoltaic based technology.

2.1.1. One-Diode Model of a Solar Cell

The circuit of the solar cell model, which consists of a photocurrent, diode, parallel resistor (leakage current), and a series resistor, is shown in Fig. 3. Consider a photovoltaic module which is equivalent to the electric circuit shown in Fig. 3 above. Using Kirchhoff current law, the current–voltage (I–V) characteristics under a solar radiation and temperature set is given as

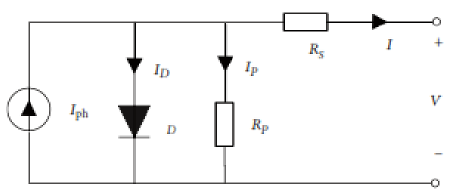

Figure 3. One-Diode PV Cell Equivalent Circuit of a PV Cell (Solar Cell).

$$I_{ph} = I + I_d + I_{sh} \tag{1}$$

Then

$$I = I_{ph} - I_d - I_{sh} \tag{2}$$

where [23],

$$I_{sh} = \frac{V + IR_s}{R_{sh}}, \quad I_d = I_o\left[\exp\left(\frac{V + IR_s}{a_f}\right) - 1\right], \quad \alpha_f = \frac{knT_c}{q}, \; I_{ph} = \left[I_{sc,ref} + k_i\left(T - T_{ref}\right)\right]\frac{S}{S_{ref}},$$

$$I_o = I_{o,ref}\left(\frac{T}{T_{ref}}\right)^3 \exp\left[\frac{E_g}{a_f}\left(\frac{1}{T_r} - \frac{1}{T}\right)\right] \; I_{o,ref} = I_{L,ref}\exp\left(\frac{-V_{oc,ref}}{a_{ref}}\right), \quad V_t = \frac{kT_c}{q}, \quad E_g = E_{go} - \frac{\alpha T^2}{T + \beta},$$

$$T_r = \left(T_{ri} - 32\right) + 273$$

i.e., we have $I = I_{ph} - I_o\left[exp\left(\frac{V+IR_S}{\alpha_f} - 1\right)\right] - \frac{V+IR_S}{R_{sh}}$

Therefore, Eq. (1) can be written as

$$I = \left[I_{sc,ref} + k_i\left(T - T_{ref}\right)\right]\frac{S}{S_{ref}} - I_{o,ref}\left(\frac{T}{T_{ref}}\right)^3 \exp\left[\frac{E_g}{a_f}\left(\frac{1}{T_r} - \frac{1}{T}\right)\right]\left[\exp\left(\frac{V_t + IR_s}{a_f}\right) - 1\right] - \frac{V_t + IR_s}{R_{sh}} \quad (3)$$

It should be pointed out that the above Eq. (3) is an implicit equation which can be easily solved analytically using Lambert W-function.

Table 1. Parameter for the Circuit Determination.

	E_{go} (T= 0 K) (eV)	$\alpha \times 10^{-4}$ (eV/k^2)	β(k)
Si	1.17	4.730	6.36
AsGa	1.52	5.405	204
InP	1.42	4.906	327

Source [23] and [24]

Table 2. Ideality Factor for Different PV Technology.

Technology	***n***
Si-mono	1.2
Si-poly	1.3
a **- Si:H**	1.8
a **- Si:H tandem**	3.3
a **- Si:H triple**	5.0
CdTe	1.5
CIS	1.5
AsGa	1.3

Source [23] and [24]

Table 1 shows the parameter for the circuit determination while Table 2 gives ideality factor for different PV technology.

The above model in Eq. (3) contains five unknown parameters, namely: I_{ph}, I, α_f, R_s, and R_{sh}. The determination of the electrical behavior of the photovoltaic module is based on these five parameters. Therefore, the five unknown parameters are needed to be found.

2.1.2. Two–Diode Model of a Solar Cell

In the two-diode model, an extra diode is attached in parallel to the circuit of single-diode model (Fig. 4). This diode is included to provide a more accurate I–V characteristics curve that considers for the difference in flow of the current at low current values due to charge combination in the semi-conductor depletion. The generalized model for N-diode is shown in Fig. 5.

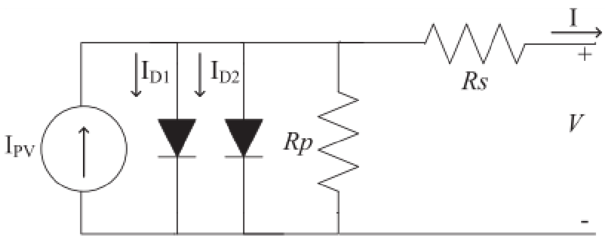

Figure 4. Equivalent Circuit of the Two-Diode Model of a Solar Cell.

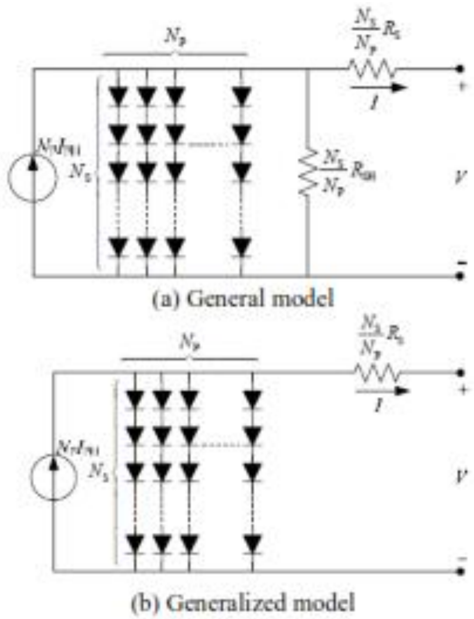

Figure 5. Equivalent Circuit Models of PV Module [25]

From Fig. 2, the output cell is written as:

$$I = I_{ph} - I_{o1}\left[\exp\left(\frac{V_t + IR_s}{\alpha_{f1}} - 1\right)\right] - I_{o2}\left[\exp\left(\frac{V_t + IR_s}{\alpha_{f2}} - 1\right)\right] - \frac{V_t + IR_s}{R_{sh}} \quad (4)$$

where

$$\alpha_{f1} = \frac{kn_1T_c}{q}, \qquad \alpha_{f2} = \frac{kn_2T_c}{q}$$

Eq. (4) can equivalently be written as

$$I=\left[I_{sc,ref}+k_i\left(T-T_{ref}\right)\right]\frac{S}{S_{ref}}-I_{o1,ref}\left(\frac{T}{T_{ref}}\right)^3\exp\left[\frac{E_g}{a_{f1}}\left(\frac{1}{T_r}-\frac{1}{T}\right)\right]\left[\exp\left(\frac{V_t+IR_s}{a_{f1}}\right)-1\right]$$
$$-I_{o2,ref}\left(\frac{T}{T_{ref}}\right)^3\exp\left[\frac{E_g}{a_{f2}}\left(\frac{1}{T_r}-\frac{1}{T}\right)\right]\left[\exp\left(\frac{V_t+IR_s}{a_{f2}}\right)-1\right]-\frac{V_t+IR_s}{R_{sh}} \qquad (5)$$

Also, the three-diode model is developed as

$$I=\left[I_{sc,ref}+k_i\left(T-T_{ref}\right)\right]\frac{S}{S_{ref}}-I_{o1,ref}\left(\frac{T}{T_{ref}}\right)^3\exp\left[\frac{E_g}{a_{f1}}\left(\frac{1}{T_r}-\frac{1}{T}\right)\right]\left[\exp\left(\frac{V_t+IR_s}{a_{f1}}\right)-1\right]$$
$$-I_{o2,ref}\left(\frac{T}{T_{ref}}\right)^3\exp\left[\frac{E_g}{a_{f2}}\left(\frac{1}{T_r}-\frac{1}{T}\right)\right]\left[\exp\left(\frac{V_t+IR_s}{a_{f2}}\right)-1\right] \qquad (6)$$
$$-I_{o3,ref}\left(\frac{T}{T_{ref}}\right)^3\exp\left[\frac{E_g}{a_{f3}}\left(\frac{1}{T_r}-\frac{1}{T}\right)\right]\left[\exp\left(\frac{V_t+IR_s}{a_{f3}}\right)-1\right]-\frac{V_t+IR_s}{R_{sh}}$$

Generally, for the N-diode model

$$I=\left[I_{sc,ref}+k_i\left(T-T_{ref}\right)\right]\frac{S}{S_{ref}}-I_{o1,ref}\left(\frac{T}{T_{ref}}\right)^3\exp\left[\frac{E_g}{a_{f1}}\left(\frac{1}{T_r}-\frac{1}{T}\right)\right]\left[\exp\left(\frac{V_t+IR_s}{a_{f1}}\right)-1\right]$$
$$-I_{o2,ref}\left(\frac{T}{T_{ref}}\right)^3\exp\left[\frac{E_g}{a_{f2}}\left(\frac{1}{T_r}-\frac{1}{T}\right)\right]\left[\exp\left(\frac{V_t+IR_s}{a_{f2}}\right)-1\right]$$
$$-I_{o3,ref}\left(\frac{T}{T_{ref}}\right)^3\exp\left[\frac{E_g}{a_{f3}}\left(\frac{1}{T_r}-\frac{1}{T}\right)\right]\left[\exp\left(\frac{V_t+IR_s}{a_{f3}}\right)-1\right]-\ldots \qquad (7a)$$
$$-I_{oN,ref}\left(\frac{T}{T_{ref}}\right)^3\exp\left[\frac{E_g}{a_{fN}}\left(\frac{1}{T_r}-\frac{1}{T}\right)\right]\left[\exp\left(\frac{V_t+IR_s}{a_{fN}}\right)-1\right]-\frac{V_t+IR_s}{R_{sh}}$$

which can be written as

$$I=\left[I_{sc,ref}+k_i\left(T-T_{ref}\right)\right]\frac{S}{S_{ref}}-\sum_{i=1}^{N}I_{oi,ref}\left(\frac{T}{T_{ref}}\right)^3\exp\left[\frac{E_g}{a_{fi}}\left(\frac{1}{T_r}-\frac{1}{T}\right)\right]\left[\exp\left(\frac{V_t+IR_s}{a_{fi}}\right)-1\right]-\frac{V_t+IR_s}{R_{sh}} \qquad (7b)$$

In the above two-diode model, seven unknown parameters, namely: I_{ph}, I_{01}, α_f, n_1, n_2, R_s, and R_{sh} are needed to be found, while for a three-diode model, there nine unknown parameters, and in general, the N-diode model has 3+2N unknown parameters, where N is the number of diode model. This therefore presents some difficulties (both in computation time and cost) in solving the model. For the sake of simplicity, one-diode model is often used, which also presents very good accurate results.

2.1.3. Determination of the Five Parameters In One-Diode Model

The five parameters corresponding to STC are designated by: $I_{ph\ ref}$, $I_{o\ ref}$, $R_{s,\ ref}$, $R_{sh,\ ref}$ and α_{ref}. The index is relative to reference condition

The I-V characteristic equations at STC are given as:

$$I = I_{ph\ \mathrm{ref}} - I_{o\ \mathrm{ref}}\left[\exp\left(\frac{I_{sc\ \mathrm{o}} R_{s\ \mathrm{ref}}}{a_{ref}}\right) - 1\right] - \frac{V + IR_{ref}}{R_{sh\ \mathrm{ref}}} \tag{8a}$$

and

$$a_{ref} = \frac{N_s A_o k T_{c\ \mathrm{ref}}}{q_{ref}} \tag{8b}$$

In order to calculate the five-reference parameter, the following conditions are adopted [27]

I. At short-circuit point: $V = 0, I = I_{sc}$

$$I_{sc\ o} = I_{ph\ \mathrm{ref}} - I_{o\ \mathrm{ref}}\left[\exp\left(\frac{I_{sc\ \mathrm{o}} R_{s\mathrm{ref}}}{a_{ref}}\right) - 1\right] - \frac{I_{sc\ \mathrm{o}} R_{ref}}{R_{sh\ \mathrm{ref}}} \tag{9}$$

II. At the open-circuit point: $I = 0, V = V_{oc}$

$$0 = I_{ph\ \mathrm{ref}} - I_{o\ \mathrm{ref}}\left[\exp\left(\frac{V_{\mathrm{oc\ ref}}}{a_{ref}}\right) - 1\right] - \frac{V_{\mathrm{oc\ ref}}}{R_{sh\ \mathrm{ref}}} \tag{10}$$

III. At maximum power point (MPP): $I = I_{am}, V = V_{mp}$

$$I_{mp\ ref} = I_{ph\ ref} - I_{o\ ref}\left[\exp\left(\frac{V_{mp\ ref} + I_{mp\ ref} R_{sh\ ref}}{a_{ref}}\right) - 1\right] - \frac{V_{mp\ ref} + I_{mp\ ref} R_{sh\ ref}}{R_{sh\ ref}} \tag{11}$$

IV. Also, at MPP, the derivative of the power with respect to the voltage is equal to zero, i.e.

$$P = VI_{ph\ ref} - VI_{o\ ref}\left[\exp\left(\frac{V + I_{ref} R_{s\ ref}}{a_{ref}}\right)\right] + VI_{o\ ref} - \frac{V^2}{R_{sh\ ref}} + \frac{V + I_{ref} R_{s\ ref}}{R_{sh\ ref}} \tag{12}$$

For

$$\left[\frac{dP}{dV}\right]_{mpp,ref} = 0$$

one arrives

$$0 = I_{ph\ ref} - I_{o\ ref}\left[\left(\frac{V}{a_{ref}} + 1\right)\exp\left(\frac{V + I_{ref} R_{s\ ref}}{a_{ref}}\right) - 1\right] - \frac{2V + I_{ref} R_{s\ ref}}{R_{sh\ ref}} \tag{13}$$

V. At the short-circuit point, the slope of the I-V curve at short circuit is given by:

$$\left(\frac{dI}{dV}\right)_{I_{sc}} = -\frac{1}{R_{sh\ ref}}, \qquad \left.\frac{dI}{dV}\right|_{V=0} = 0 \tag{14}$$

Recall

$$I = I_{ph\ ref} - I_{o\ ref}\left[\exp\left(\frac{V + IR_{ref}}{a_{ref}}\right) - 1\right] - \frac{V + IR_{s\ ref}}{R_{sh\ ref}} \tag{15}$$

For

$$\left.\frac{dI}{dV}\right|_{V=0} = 0$$

One arrives at

$$0 = -I_{o\ ref}\left[\frac{1}{a_{ref}} + \frac{R_{ref}}{a_{ref}}\frac{dI}{dV}\right]\exp\left(\frac{V + IR_{ref}}{a_{ref}}\right) - \left(\frac{1}{R_{sh\ ref}} + \frac{R_{s\ ref}}{R_{sh\ ref}}\frac{dI}{dV}\right)\frac{V + IR_{s\ ref}}{R_{sh\ ref}} \tag{16}$$

Thus, the five parameters ($I_{ph\ ref}$, $I_{o\ ref}$, $R_{s,\ ref,}$, $R_{sh,\ ref,}$ and α_{ref}) can be obtained simultaneously solving these equations below by using iterative method like Newton-Raphson's method to solve the system of non-linear equations below:

$$I_{sc\ o} = I_{ph\ ref} - I_{o\ ref}\left[\exp\left(\frac{I_{sc\ o}R_{sref}}{a_{ref}}\right) - 1\right] - \frac{I_{sc\ o}R_{ref}}{R_{sh\ ref}} \tag{17a}$$

$$0 = I_{ph\ ref} - I_{o\ ref}\left[\exp\left(\frac{V_{oc\ ref}}{a_{ref}}\right) - 1\right] - \frac{V_{oc\ ref}}{R_{sh\ ref}} \tag{17b}$$

$$I_{mp\ ref} = I_{ph\ ref} - I_{o\ ref}\left[\exp\left(\frac{V_{mp\ ref} + I_{mp\ ref}R_{sh\ ref}}{a_{ref}}\right) - 1\right] - \frac{V_{mp\ ref} + I_{mp\ ref}R_{sh\ ref}}{R_{sh\ ref}} \tag{17c}$$

$$I_{ph\ ref} = I_{o\ ref}\left[\frac{V_{mpp\ ref}}{a_{ref}}\left(1 - \frac{I_{mpp\ ref}R_{s\ ref}}{V_{mpp\ ref}}\right)\right]\exp\left(\frac{V_{mpp\ ref} + I_{mpp\ ref}R_{s\ ref}}{a_{ref}}\right) - \frac{V_{mpp\ ref}}{R_{sh\ ref}}\left(1 - \frac{I_{mpp\ ref}R_{s\ ref}}{V_{mpp\ ref}}\right) \tag{17d}$$

$$0 = -I_{o\ ref}\left[\frac{1}{a_{ref}} + \frac{R_{ref}}{a_{ref}}\frac{dI}{dV}\right]\exp\left(\frac{V + IR_{ref}}{a_{ref}}\right) - \left(\frac{1}{R_{sh\ ref}} + \frac{R_{s\ ref}}{R_{sh\ ref}}\frac{dI}{dV}\right)\frac{V + IR_{s\ ref}}{R_{sh\ ref}} \tag{17e}$$

2.1.4. Development of Current–Voltage Characteristics of Solar Panel

The current–voltage (I–V) characteristics of a solar panel under a solar radiation and temperature set is given as:

$$I_{panel} = N_p I_{ph,cell} - I_{o,cell}\left[\exp\left(\frac{V + I_{panel}R_s}{N_s a_f}\right) - 1\right] - \frac{V_{panel} + I_{panel}R_s}{R_{sh}} \tag{18}$$

where

$$a_{ref} = \frac{2V_{m/ph,ref} - V_{oc,ref}}{\dfrac{I_{sc,ref}}{I_{sc,ref} - I_{m/ph,ref}} + In\left(1 - \dfrac{\mathrm{I}_{m/ph,ref}}{I_{sc,ref}}\right)}, \qquad I_L = \frac{S}{S_{ref}}\left[I_{L,ref} + \mu_{I,sc}\left(T_c - T_{c,ref}\right)\right]$$

$$E_{g,ref} = 1.12eV, \quad I_{L,ref} = I_{sc,ref} = 2.664A$$

The electric PV power output in DC, taking into account the efficiency of conversion to electric energy is

$$P_{PV} = \eta_c I_{panel} V_{panel} \tag{19}$$

While under the dynamic condition

$$P_{PV}(t) = \eta_c I_{panel}(t) V_{panel}(t) \tag{20}$$

Where η_c is the efficiency of conversion to DC.

$$\eta_c = \frac{\left\{\begin{array}{l} \sigma\left(T_{panel}^4 - T_{sky}^4\right)\left\{1 + \left(\dfrac{1}{3}\right)\left(\dfrac{T_{Envr.}}{T_{Sun}}\right)^4 - \left(\dfrac{4}{3}\right)\left(\dfrac{T_{Envr.}}{T_{Sun}}\right)\right\} \\ -\left\{\sigma\left[T_{panel}^4 - T_{Sky}^4 - \dfrac{4}{3}T_{Envr.}\left(T_{panel}^3 - T_{Sky}^3\right)\right]\right\} \\ -\dfrac{4T_E}{3}\left\{\dfrac{4}{3}\left(T_{panel}^3 - T_{Sky}^3\right) - \dfrac{\sigma\left(T_{panel}^4 - T_{sky}^4\right)}{T_{Sun}}\right\} \end{array}\right\}}{\sigma\left(T_{panel}^4 - T_{sky}^4\right)} \tag{21}$$

2.2. Modeling the Power Generation by the Wind Turbine

Power extraction from the air stream by the turbine under constant wind speed is given as

$$P_{WT} = \frac{1}{2}\rho A C_p V_w^3 \tag{22}$$

The power extracted from the air stream by turbine when the wind speed varies with time is given as

$$P_{WT} = \frac{1}{2}\rho A C_p V_w^3(t) \tag{23}$$

where

$$\omega = \frac{2\pi}{T},\ V_w = V_{\min} + V_{\max} \sin \omega t$$

V_{max} is the maximum current speed at the surface

ω is the angular velocity of the wind

T is the period of the cycle.

In the above Eqs. (22) and (23), C_p is the fraction of the upstream wind power which is captured by the rotor blades, and it has theoretical maximum value of 0.59. It is often called power coefficient of the rotor or the rotor efficiency in practical designs. The maximum achievable C is between 0.4 and 0.5 for high-speed, two – blade turbines and 0.2 and 0.4 for slow speed turbines with more blades. The power coefficient has been shown to be dependent on tip speed ratio, λ (the ratio between the blade tip speed V and product of the wind speed upstream of the rotor v), and the blade angle, θ. Based on Sobamowo et al. [26],

$$C_p = 0.73\left\{151\left(\frac{1}{\lambda - 0.02\theta} + \frac{0.003}{\theta^3 + 1}\right) - 0.58\theta - 0.002\theta^{2.14} - 3.12\right\} e^{18.4\left(\frac{1}{\lambda - 0.02\theta} + \frac{0.003}{\theta^3 + 1}\right)} \tag{24}$$

The power extracted from the wind under constant wind speed is given as

$$P_{WT} = 0.365\rho A V_w^3 \left\{151\left(\frac{1}{\lambda - 0.02\theta} + \frac{0.003}{\theta^3 + 1}\right) - 0.58\theta - 0.002\theta^{2.14} - 3.12\right\} e^{18.4\left(\frac{1}{\lambda - 0.02\theta} + \frac{0.003}{\theta^3 + 1}\right)} \tag{25}$$

while under the time-variant wind speed condition

$$P_{WT} = 0.365\rho A V_w^3(t) \left\{151\left(\frac{1}{\lambda - 0.02\theta} + \frac{0.003}{\theta^3 + 1}\right) - 0.58\theta - 0.002\theta^{2.14} - 3.12\right\} e^{18.4\left(\frac{1}{\lambda - 0.02\theta} + \frac{0.003}{\theta^3 + 1}\right)} \tag{26}$$

Power produced (power output) by the wind turbine under constant wind speed is

$$P_{WT} = 0.365\eta_{fmec}\eta_{gf}\eta_{smb}\rho A V_w^3 \left\{151\left(\frac{1}{\lambda - 0.02\theta} + \frac{0.003}{\theta^3 + 1}\right) - 0.58\theta - 0.002\theta^{2.14} - 3.12\right\} e^{18.4\left(\frac{1}{\lambda - 0.02\theta} + \frac{0.003}{\theta^3 + 1}\right)}$$

where η_{fmec} and η_{gf} are mechanical friction and generator efficiencies respectively and the efficiency speed multiplication box is η_{smb}

while under the dynamic condition

$$P_{WT} = 0.365\eta_{fmec}\eta_{gf}\eta_{smb}\rho A V_w^3(t) \left\{151\left(\frac{1}{\lambda - 0.02\theta} + \frac{0.003}{\theta^3 + 1}\right) - 0.58\theta - 0.002\theta^{2.14} - 3.12\right\} e^{18.4\left(\frac{1}{\lambda - 0.02\theta} + \frac{0.003}{\theta^3 + 1}\right)}$$

2.3. Modeling Battery–Ultracapacitor Hybrid for Solar and Wind Applications

In this section, mathematical models are developed for battery and ultra-capacitor for a hybrid solar wind power generation.

2.3.1. Modeling of the Battery

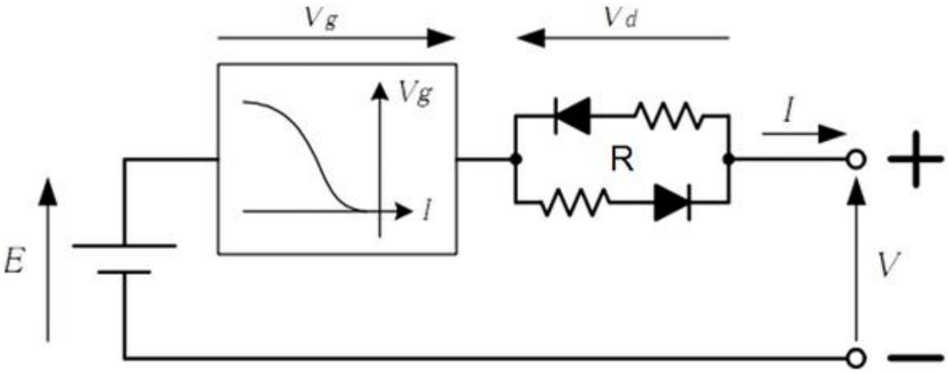

Figure 6. A Simplified Lead-Acid Battery Equivalent Electric Model.

2.3.1.1. Model for the Battery Capacity

The battery capacity is not constant and is strongly dependent on discharge current I and the electrolyte temperature. Following the simplified Lead-acid battery equivalent electric model shown in Fig. 6, at fixed discharged currents, the variation of capacity is given by:

$$C(I,\theta) = C_o(I)\left[1-\frac{\theta}{\theta_f}\right]^n \tag{29}$$

The empirical result of $C_o(I)$ is given as

$$C_o(I) = \frac{k_c C_o}{1+(k_c-1)\left(\frac{I}{I'}\right)^m} \tag{30}$$

which implies that:

$$C(I,\theta) = \frac{k_c C_o \left(1-\frac{\theta}{\theta_f}\right)^n}{1+(k_c-1)\left(\frac{I}{I'}\right)^m} \tag{31}$$

Also,

$$C(0,\theta) = k_c C_o \left(1-\frac{\theta}{\theta_f}\right)^n \tag{32}$$

2.3.2. Model for the State of Charge of the Battery

The state of charge (SOC) is the ratio of the capacity remaining in the battery to the maximum capacity of the battery at a given temperature.

$$SOC = \frac{C(0,\theta) - Q_e}{C(0,\theta)} = 1 - \frac{Q_e}{C(0,\theta)} \tag{33}$$

which gives

$$SOC = 1 - \frac{Q_e \theta_f^n}{k_c C_o \left(\theta_f - \theta\right)^n} \tag{34}$$

2.3.3. Model for the Depth of Charge of the Battery

This is the ratio of the capacity remaining in the battery to the maximum capacity of the battery with reference to the actual discharge regime.

$$DOC = 1 - \frac{Q_e}{C\left(I_{avg},\theta\right)} \tag{35}$$

$$DOC = \frac{1 - \dfrac{Q_e}{k_c C_o \left(1 - \dfrac{\theta}{\theta_f}\right)^n}}{1 + \left(k_c - 1\right)\left(\dfrac{I_{avg}}{I'}\right)^m} \tag{36}$$

$$DOC = 1 - \frac{Q_e \left[1 + \left(k_c - 1\right)\left(\dfrac{I_{avg}}{I'}\right)^m\right]}{k_c C_o \left(1 - \dfrac{\theta}{\theta_f}\right)^n} \tag{37}$$

2.3.4. Model for the Ultra-Capacitor

Consider the equivalent circuit of an ultra-capacitor circuit shown in Fig. 7

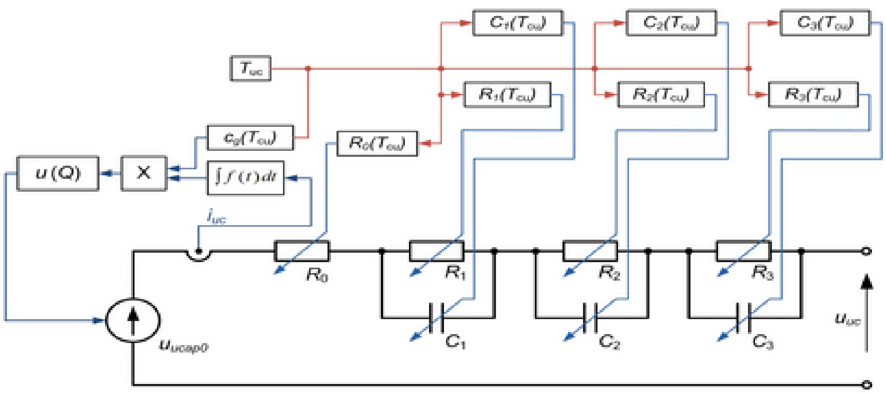

Figure 7. An Equivalent Circuit of an Ultra-Capacitor Circuit.

Voltage drop across resistor, $V_R = R_T I$ (38a)

Voltage drop across capacitor, $V_C = q/C$ (38b)

Applied voltage, $V = V_R + V_C$ (38c)

For a two ultracapacitor model, using Kirchhoff's voltage law and Kirchhoff's current law, the following equation was obtained:

$$\frac{dI_2(t)}{dt} = \frac{V_a}{CR_1R_2} - \frac{1}{C}\left[\frac{1}{R_1} + \frac{1}{R_2}\right] I_2(t) \quad (39)$$

Solving the above Eq. (39) applying Laplace transform, one arrives at

$$I_2(t) = I_o e^{-\frac{R_2+R_1}{CR_2R_1}t} + \frac{V_a}{R_1+R_2}\left[1 - e^{-\left(\frac{R_2+R_1}{CR_2R_1}\right)t}\right] \quad (40)$$

Using Kirchhoff's voltage law

$$R_1 I_1 + R_2 I_2 = V_a \quad (41)$$

Using the current's law,

And

$$I_1 = I_2 + I_3 \quad (42)$$

But

$$I_1(t) = \frac{V_a - I_2R_2}{R_1} = \frac{V_a}{R_1} - \frac{R_2}{R_1} I_2(t) \quad (43)$$

Therefore,

$$I_1(t) = \frac{V_a}{R_1} - \frac{R_2}{R_1}\left[I_o e^{-\frac{R_2+R_1}{CR_2R_1}t} + \frac{V_a}{R_1+R_2}\left[1 - e^{-\left(\frac{R_2+R_1}{CR_2R_1}\right)t}\right]\right] \quad (44)$$

From Equ. (42)

$$I_3(t) = I_1(t) - I_2(t)$$

Therefore,

$$I_3(t) = I_o e^{-\left(\frac{R_2+R_1}{CR_2R_1}\right)t} + \frac{V_a}{R_1+R_2}\left[1 - e^{-\left(\frac{R_2+R_1}{CR_2R_1}\right)t}\right] - \frac{V_a}{R_1} + \frac{R_2}{R_1}\left[I_o e^{-\left(\frac{R_2+R_1}{CR_2R_1}\right)t} + \frac{V_a}{R_1+R_2}\left[1 - e^{-\left(\frac{R_2+R_1}{CR_2R_1}\right)t}\right]\right] \quad (45)$$

recall,

$$V_C = V_a - V_R = V_a - R_1\left[\frac{V_a}{R_1} - \frac{R_2}{R_1}\left[I_o e^{-\left(\frac{R_2+R_1}{CR_2R_1}\right)t} + \frac{V_a}{R_1+R_2}\left[1-e^{-\left(\frac{R_2+R_1}{CR_2R_1}\right)t}\right]\right]\right] \tag{46}$$

$$V_C = R_2\left[I_o e^{-\left(\frac{R_2+R_1}{CR_2R_1}\right)t} + \frac{V_a}{R_1+R_2}\left[1-e^{-\left(\frac{R_2+R_1}{CR_2R_1}\right)t}\right]\right] \tag{47}$$

and

$$V_R = R_2\left[I_o e^{-\left(\frac{R_2+R_1}{CR_2R_1}\right)t} + \frac{V_a}{R_1+R_2}\left[1-e^{-\left(\frac{R_2+R_1}{CR_2R_1}\right)t}\right]\right] - V_a \tag{48}$$

The total power output form the solar and wind hybrid system is given by

$$P_{TOTAL} = P_{PV} + P_{WT} \tag{49}$$

Substituting Eqs.(19) and (27) and into Eq. (49), for under constant wind speed, one arrives at

$$P_{TOTAL} = \eta_c I_{panel} V_{panel} + 0.365\eta_{fmec}\eta_{gf}\eta_{smb}\rho A V_w^3\left\{151\left(\frac{1}{\lambda-0.02\theta}+\frac{0.003}{\theta^3+1}\right) - 0.58\theta - 0.002\theta^{2.14} - 3.12\right\}e^{18.4\left(\frac{1}{\lambda-0.02\theta}+\frac{0.003}{\theta^3+1}\right)} \tag{50}$$

where

$$I_{panel} = N_p I_{ph,cell} - I_{o,cell}\left[\exp\left(\frac{V + I_{panel}R_s}{N_s a_f}\right) - 1\right] - \frac{V_{panel} + I_{panel}R_s}{R_{sh}}$$

$$a_{ref} = \frac{2V_{m/ph,ref} - V_{oc,ref}}{\frac{I_{sc,ref}}{I_{sc,ref} - I_{m/ph,ref}} + In\left(1 - \frac{I_{m/ph,ref}}{I_{sc,ref}}\right)}, \qquad I_L = \frac{S}{S_{ref}}\left[I_{L,ref} + \mu_{I,sc}\left(T_c - T_{c,ref}\right)\right]$$

$$E_{g,ref} = 1.12eV, \quad I_{L,ref} = I_{sc,ref} = 2.664A$$

While when one substitutes Eqs.(20) and (28) and into Eq. (49), for under the time-dependent wind speed, it gives

$$P_{TOTAL} = \eta_c I_{panel}(t) V_{panel}(t) + P_{WT} = 0.365\eta_{fmec}\eta_{gf}\eta_{smb}\rho A V_w^3(t)\left\{151\left(\frac{1}{\lambda-0.02\theta}+\frac{0.003}{\theta^3+1}\right) - 0.58\theta - 0.002\theta^{2.14} - 3.12\right\}e^{18.4\left(\frac{1}{\lambda-0.02\theta}+\frac{0.003}{\theta^3+1}\right)} \tag{51}$$

Finally, the hybrid system energy conversion efficiency for harnessing energy from solar and wind is given by;

For the static condition

$$\eta_{Hybrid} = \frac{\eta_{inverter} V_{out} I_o}{\eta_c I_{panel} V_{panel} + 0.365 \eta_{fmec} \eta_{gf} \eta_{smb} \rho A V_w^3 \left\{151\left(\frac{1}{\lambda - 0.02\theta} + \frac{0.003}{\theta^3 + 1}\right) - 0.58\theta - 0.002\theta^{2.14} - 3.12\right\} e^{18.4\left(\frac{1}{\lambda - 0.02\theta} + \frac{0.003}{\theta^3 + 1}\right)}} \quad (52)$$

And under the dynamic condition

$$\eta_{Hybrid} = \frac{\eta_{inverter} V_{out}(t) I_o(t)}{\eta_c I_{panel}(t) V_{panel}(t) + P_{WT} = 0.365 \eta_{fmec} \eta_{gf} \eta_{smb} \rho A V_w^3(t) \left\{151\left(\frac{1}{\lambda - 0.02\theta} + \frac{0.003}{\theta^3 + 1}\right) - 0.58\theta - 0.002\theta^{2.14} - 3.12\right\} e^{18.4\left(\frac{1}{\lambda - 0.02\theta} + \frac{0.003}{\theta^3 + 1}\right)}} \quad (53)$$

The standard test conditions (STC) used by manufacturers of the PV modules to measure data laid out on the data sheet is given by:

Irradiance (solar insolation)	1000 W/m^2
Sun temperature	6000 K
Cells temperature, T_c	298 K
Air mass number	1.5

3. RESULTS AND DISCUSSION

The developed models for the hybrid system under static and time-variant wind speeds are simulated, where the input independent parameters are defined and other dependent parameters were calculated and integrated in the system of equations. The nonlinear equations were solved numerically until the solutions reached acceptable iteration errors. The PV solar system used in this simulation has two panels array has 240 W output estimated at irradiance of 1000 W/m^2 with an open circuit current of 15.14 A and open circuit volt of 21.7 V. The module efficiency and cell temperature are 12.1 % and 25 °C, respectively. The simulated results are given in Fig. 8-21.

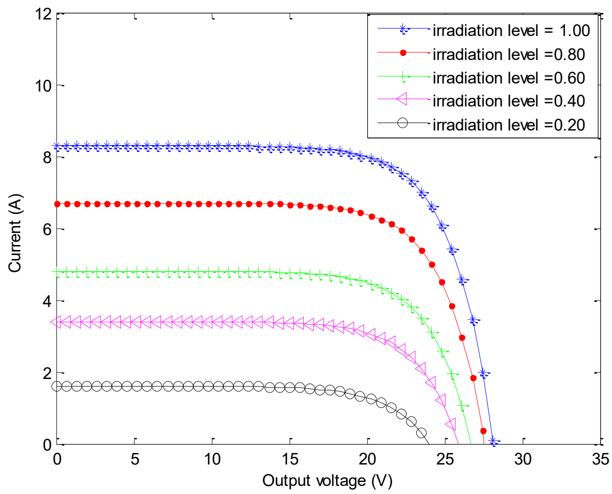

Figure 8. I-V Curve of Two-Diode Model of PV Module for Several Irradiation Levels at Temperature 28°C.

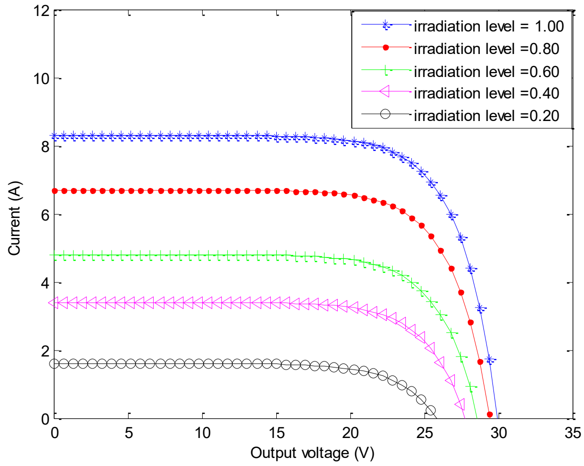

Figure 9. I-V Curve of Two-Diode Model of PV Module for Several Irradiation Levels at Temperature 35°C.

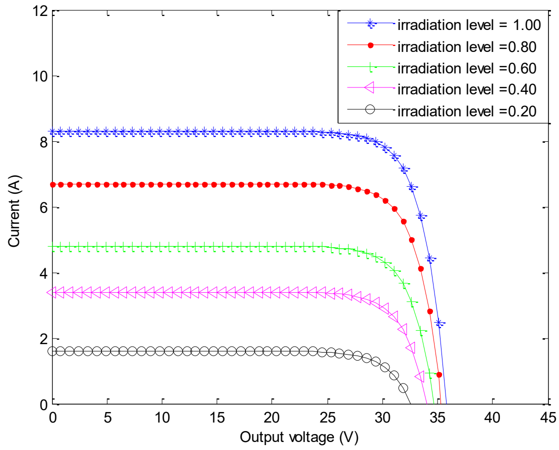

Figure 10. I-V Curve of Two-Diode Model of PV Module for Several Irradiation Levels at Temperature of 56°C.

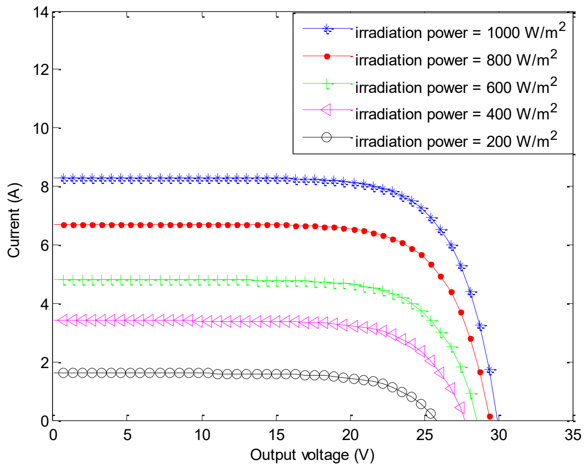

Figure 11. I-V Curve of Two-Diode Model of PV Module for Several Irradiation Powers at Temperature 28°c.

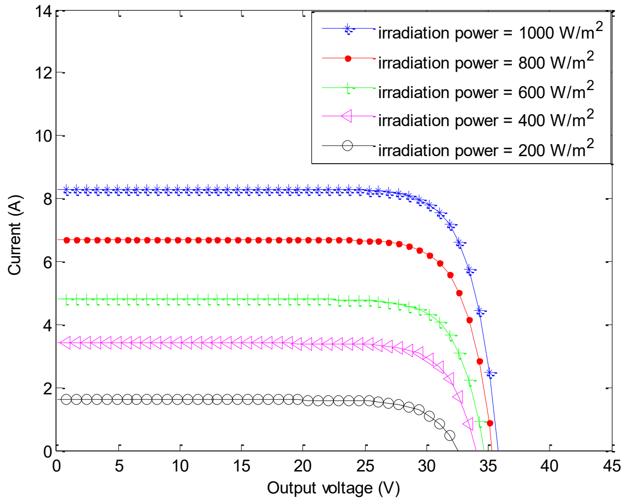

Figure 12. I-V Curve of Two-Diode Model of PV Module for Several Irradiation Levels at Temperature of 35°C.

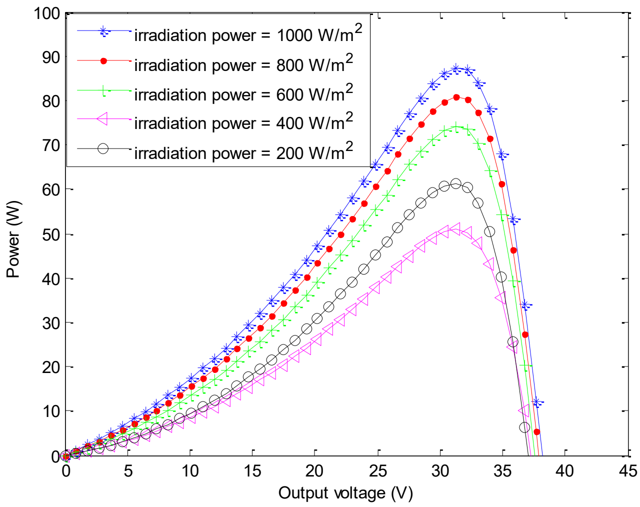

Figure 13. P-V Curve of Two-Diode Model of PV Module for Several Irradiation Levels at Temperature 28°C.

By varying the irradiation (200 W/m^2, 400 W/m^2, 600 W/m^2, 800 W/m^2, 1000 W/m^2) and solar temperature, Figs. 8-14 show results under these conditions on I-V and P-V characteristics. It is clear that current generated by the incident light depends on irradiation, the higher the irradiation, the greater the current. On the other hand, voltage is staying almost constant and it is not going to. The influence of irradiation on maximum power point is clear, the higher the irradiation, the major of the maximum power point will be light is going to stay constant although it increases slightly while the voltage decreases. The effect of the temperature increase decreases voltage and power. The Figures show the influence of both the irradiation and the temperature, we can remark that the I-V and P-V curves are similar to these of the irradiation influence, with slightly higher values of power; the effect of the temperature in this case is almost ignored. The I-V and P-V curves of a solar cell are highly dependent on the solar irradiation values.

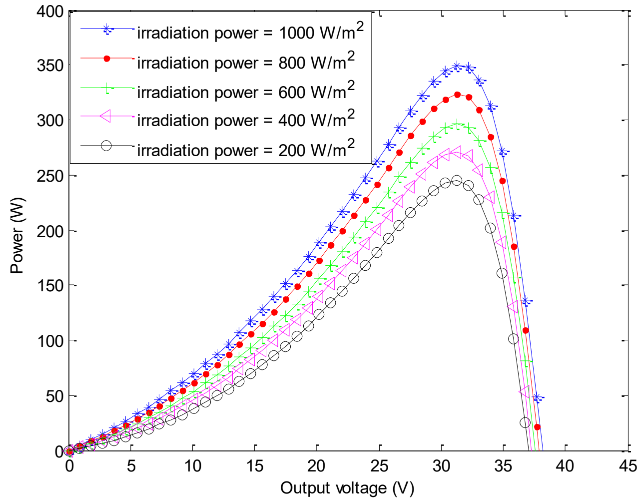

Figure 14. I-V Curve of Two-Diode Model of PV Module for Several Irradiation Levels at Temperature 56°c.

It is very clear that current generated increases with increasing solar irradiance, and maximum output power (P) also increases. The solar irradiation, as a result of the environmental changes keeps on fluctuating, but control mechanisms are available that can track this change and can alter the working of the solar cell to meet the required load demands. The higher is the solar irradiation, higher would be the solar input to the solar cell, and hence power magnitude would increase for the same voltage value. With increase in the solar irradiation, the open circuit voltage (V) increases. This is due to the fact that, when more sunlight incidents on to the solar cell, the electrons are supplied with higher excitation energy, thereby increasing the electron mobility and thus more power is generated.

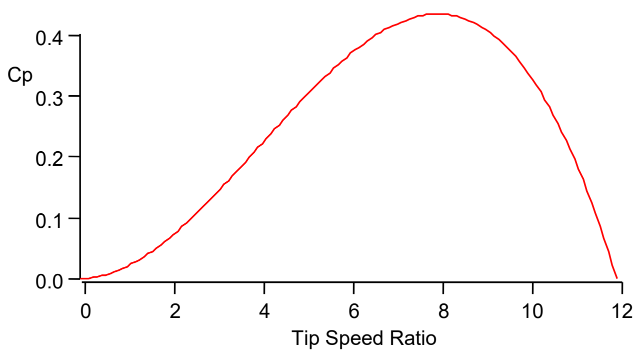

Figure 15. Power coefficient variation with tip speed ratio for wind turbine.

Fig. 15 shows the variation of power coefficient with the tip speed ratio.

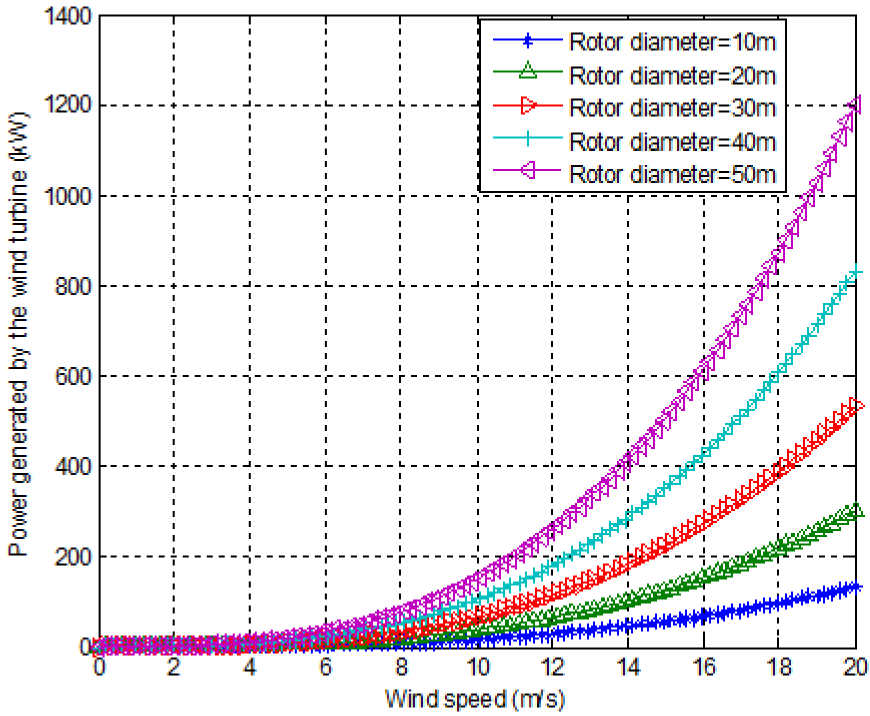

Figure 16. Effects of Rotor Diameter and Speed on the Power Generation by the Wind Turbine for Constant Power Coefficient.

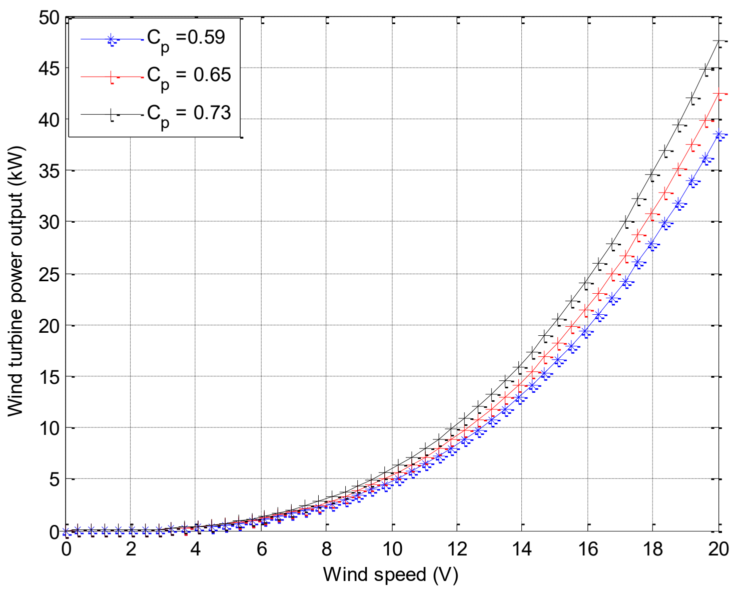

Figure 17a. Effects of Wind Speed Coefficient on the Power Generated by the Wind Turbine.

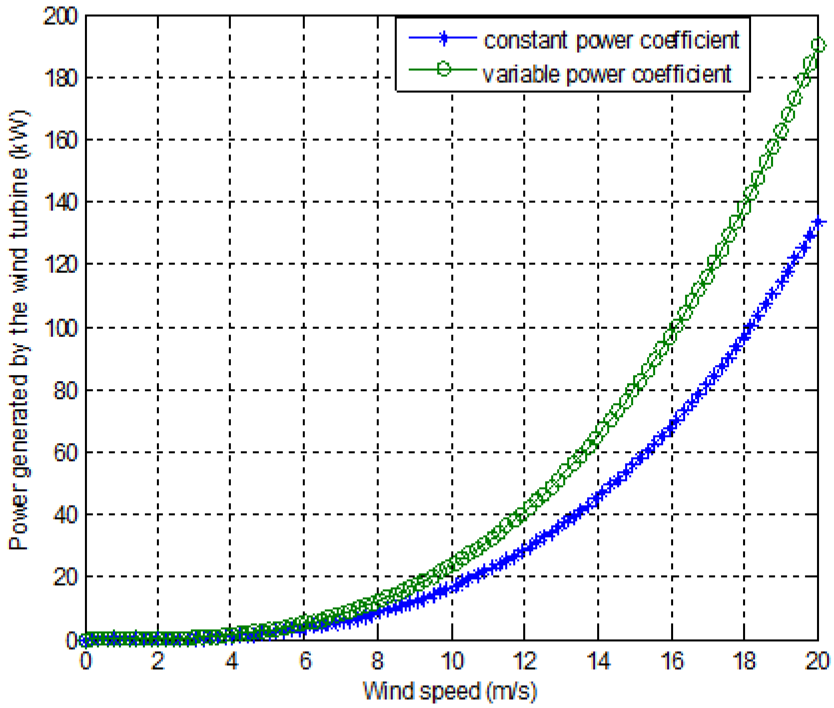

Figure 17. Effects of Power Coefficient and Speed on the Power Generated by the Wind Turbine.

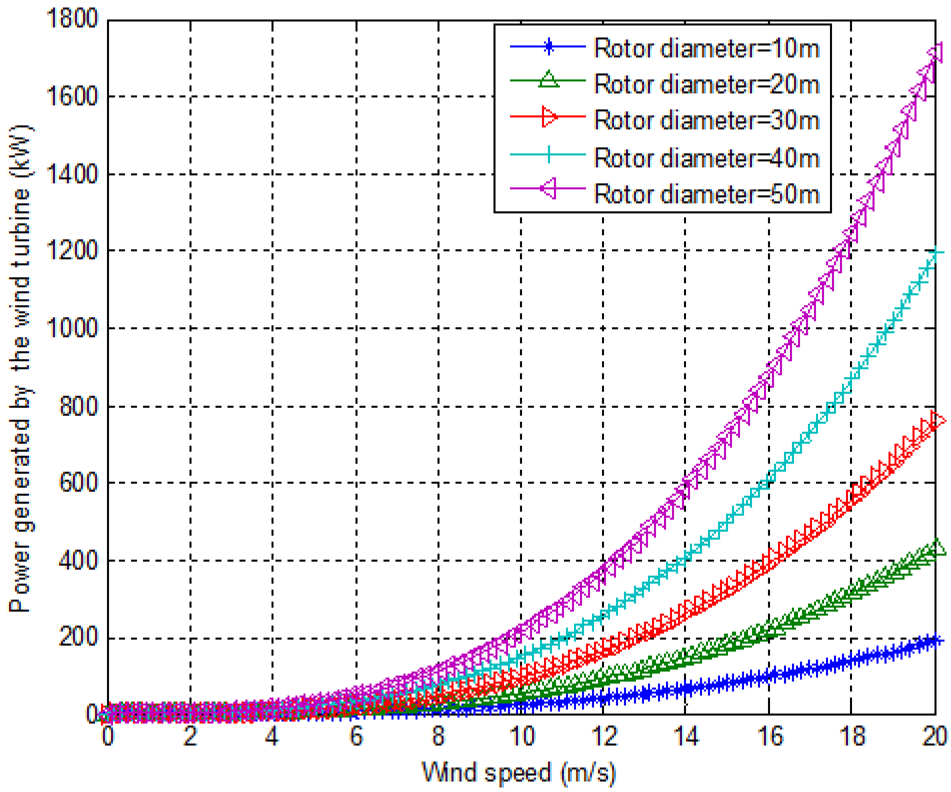

Figure 18. Effects of Rotor Diameter and Speed on the Power Generated by the Wind Turbine for Variable Power Coefficient.

Effects of power coefficient, wind speed, and the rotor diameter on the power genrated by the wind turbine are shown in Fig. 15-18. From the results, it could be seen that wind speed and rotor diameter increase the power generation by the wind turbine. It is implied for the figures that the higher wind speed results in higher energy conversion efficiency and produces more power output. However, for the wind turbine under investigation, the minimum starting wind speed is 2.5 m/s, at this particular condition, the power output and conversion efficiency are significantly low and economically viable. However, a techno-economic analysis is required for achieving optimum performance of the wind turbine with the optimum cost of the system.

Theoretically, it has been established that the maximum power generated by the wind turbine is at Betz power coefficient of 0.59. Beyond this point, with increasing the wind speed the power generated decreases. However, it is shown in Fig. 15 that wind turbine in the present investigation operates at maximum capacity with Betz coefficient of 0.42.

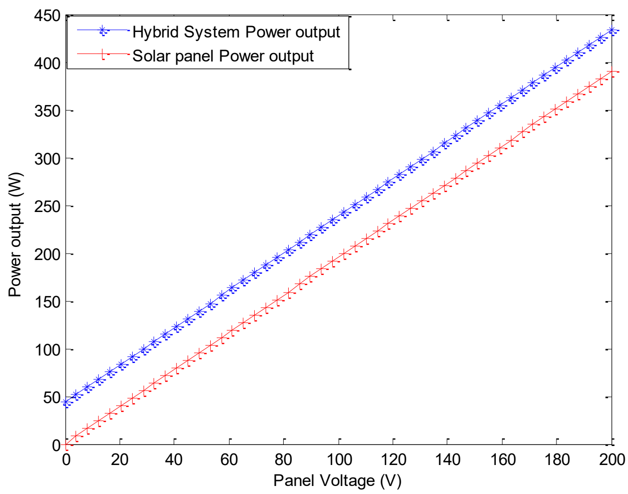

Figure 19. Effects of Panel Voltage on the Power Generated by the PV.

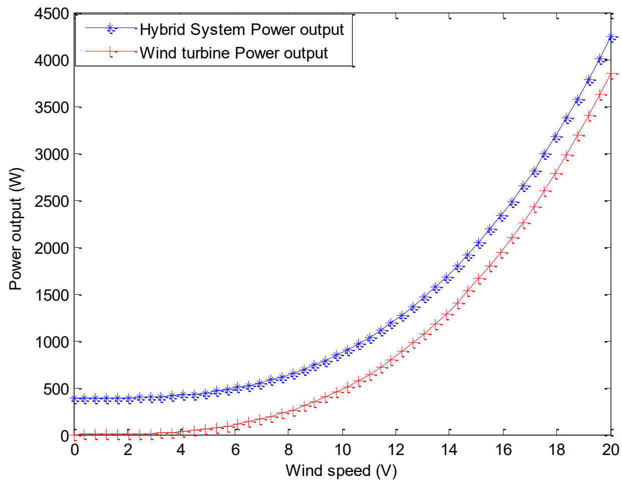

Figure 20. Effects of Wind Speed on the Power Generated by the Wind Turbine.

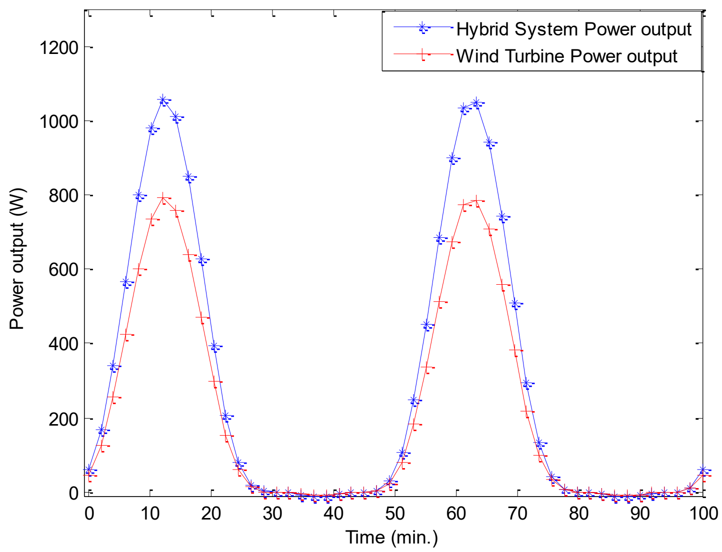

Figure 21. Effects Time-Variation Wind Speed on the Power Generated by the Hybrid and Wind Power Systems.

While Figs. 19 and 20 show the effects of panel voltage and wind speed on the power generated by solar panel and the wind turbine, respectively, Fig. 21 shows the effect of time-variation or periodic variation, in the wind speed on the wind and hybrid power system is shown in Fig. 19. It could be stated, as shown, that the hybridization of the solar-wind power system produced more and enhanced power than the solely wind or solar power system. Although the present work focuses on developing mathematical models for the various components involving in the power generation in a smart grid-connected hybrid solar-wind energy conversion system with an incorporated ultracapacitor, the work has also demonstrated that since the standalone solar photovoltaic energy system cannot provide reliable power during non-sunny days and the standalone wind system cannot meet the constant load demands due to significant fluctuations in the magnitude of wind speeds throughout the year. Therefore, energy storage systems will be required for each of these systems in order to satisfy the power demands. usually storage system is expensive, and the size has to be reduced to a minimum possible for the renewable energy system to be cost effective. Hybrid power systems can also be used to reduce energy storage requirements. By integrating and optimizing the solar photovoltaic and wind systems, the reliability of the systems can be improved and the unit cost of power can be minimized. With these systems, one can generate, store, and use the power as and when required and also for rural electrification.

4. CONCLUSION

In this work, mathematical models have been developed for power generation in a smart grid-connected hybrid solar-wind energy conversion system with an incorporated ultracapacitor. The mathematical models are developed for various components of the system. Also, the models were simulated, and effects of various parameters on the power generation and energy quality of the intelligent hybrid system are investigated. From the research, it was indicated that the higher wind speed results in higher energy conversion efficiency and produces more power output. It was established that higher irradiance will result in higher energy conversion efficiency. Therefore, the solar panels will be more efficient to operate at sites with higher irradiance. Also, it is established that the hybridization of the solar-wind power system produced more and enhanced power than the solely wind or solar power system.

By integrating and optimizing the solar photovoltaic and wind systems, the reliability of the systems can be improved, and the unit cost of power can be minimized. Although the hybrid power systems can be used to reduce energy storage requirements, it is recommended that efficient energy storage systems should be used for each of these systems in order to satisfy the power demands. It is hoped that the present study will assist in the optimization of the system for power generation.

Conflicts of Interest

The authors declare that there is no conflict of interest regarding the publication of this paper.

Nomenclature

a – P-N junction ideality factor parameter (1 – 5)
a – Thermal potential of the cell
a_f – Modified ideality factor
A_c – Thermal voltage timing completion factor (v)
C_{PV} – The overall heat capacity area (J/°C m^2)
E_g – Band gap of the material
I – Local current (A)
I – Output current of PV cell
I_d – Current through the diode
$I_{L,ref}$ or $I_{ph, ref}$ – Light current at the reference condition (A)
I_L–Light current (A) = I_{ph}
$I_{m/p}$ – Current at the max power point (A)
$I_{m/p, ref}$ – Max.power point current (A)
I_o – Reverse saturation current of the diode
I_o – Saturation current (A)
$I_{o, ref}$ – Saturation current at the reference condition (A)
I_{ph} – Photocurrent
$I_{Sc, ref}$ – Short circuit current at reference (A)
I_{sh} – Current through the shunt resistor
k – Boltzmann's constant (1.38×10^{-23} J/kg)
K – Boltzmann's constant (1.38066×10^{-23})
n – Ideality factors of the diode (typically, 1 – 2 for polycrystalline)
N_s – Number of cells in series
N_s – Number of cells in series of the PV module
q – Electron charge (1.602×10^{-19}C)
q – Electron charge (1.60218×10^{-19} C)
P_{mpp} maximum power point
R_p – Cell intrinsic shunt or parallel resistance
R_s – Series resistance
R_s – Series resistance (Ω)
R_{sh} – Shunt resistance
S – Solar radiation (W/m^2)
S or G – Irradiance (W/m^2)
S_{ref} – Solar radiation at reference (1000W/m^2)
T_c – PV cell temp
T_c – Temp o the cell
$T_{c, ref}$ – Reference temp of PV cell (25°C)
V – Output voltage (V)
$V_{m/p}$ – Voltage at the max power point (V)
$V_{m/p, ref}$ – Max.power point voltage (V)
$V_{oc, ref}$ – Open circuit voltage of the PV module (V)
V_{panel} – Voltage across panel

$\mu_{I,Sc}$ – Temp current coefficient (A/^{0}C)
$\mu_{I,Sc}$ – Temp coefficient at short circuit (A/k)
η - efficiency

References

[1] H. C. Chen, J. C. Qiu and C. H. Liu. Dynamic Modeling and Simulation of Renewable Energy Based Hybrid Power Systems, *Electric Utility Deregulation and Restructuring and Power Technologies*, Taichung, 2008, pp.2803-2809.

[2] H. H. El-Tamaly and A. A. E. Mohammed. Modeling and Simulation of Photovoltaic/Wind Hybrid Electric Power System Interconnected with Electrical Utility. *Power System Conference*, Middle-East, 2008, pp. 645-649.

[3] L. A. de Souza Ribeiro, O. R. Saavedra, S. L. de Lima, J. Gomes de Matos. "Isolated Micro-Grids with Renewable Hybrid Generation: The Case of Lençóis Island,"*IEEE Trans. on Sustainable Energy*, vol. 2, no.1, pp. 1-11, 2011

[4] F. Valenciaga and P. F. Puleston. Supervisor Control for a Stand-Alone Hybrid Generation System using Wind and Photovoltaic Energy,"*IEEE Trans.* on *Energy Conversion*, vol. 20, no. 2, pp.398-405, 2005

[5] C. Wang, and M. H. Nehrir. "Power Management of a Stand-alone Wind/photovoltaic/fuel cell Energy ystem," *IEEE Trans. on Energy Conversion*, vol. 23, no. 3, September 2008, pp. 957-967.

[6] G. Li, Y. Chen and T. Li. The Realization of Control Subsystem in the Energy Management of Wind/Solar Hybrid Power System," *Power Electronics Systems and Applications*, China, May 2009, pp.1-4.

[7] H. Yang, Z. Wei and L. Chengzh. Optimal design and technoeconomic Analysis of a Hybrid Solar-Wind Power Generation System," *Applied Energy*, vol. 86, pp. 163-169, 2009.

[8] S. Dihrab and K. Sopian. Electricity generation of hybrid PV/wind systems in Iraq. *Renewable Energy*, vol. 35, pp. 1303-1307, 2010.

[9] J. Y. Reichling and F. A. Kulacki. Utility scale hybrid wind-solar thermal electrical generation: a case study for Minnesota," *Energy*, vol. 33, pp.626-638, 2008.

[10] O. Ekren, B. Y. Ekren and B. Ozerdem. Break-even analysis and size optimization of a PV/wind hybrid energy conversion system with battery storage – A case study. *Applied Energy*, vol.86, pp. 1043-1054, 2009.

[11] S. K. Kim, J. H. Jeon, C. H. Cho, E. S. Kim, and J. B. Ahn. Modeling and Simulation of a Grid-connected PV Generation System for Electromagnetic Transient Analysis. *Solar Energy*, vol.83, pp. 664678, 2009.

[12] N. Chayawatto, K. Kirtikara, V. Monyakul, C. Jivacate and D. Chenvidhya. DC–AC Switching Converter Modelings of a PV grid-connected System under islanding phenomena. *Renewable Energy*, vol. 34, pp. 2536-2544, 2009.

[13] O. C. Onara, M. Uzunoglua and M. S. Alam. Dynamic Modeling, Design and Simulation of a Wind/Fuel Cell/Ultra-Capacitor-based Hybrid Power Generation System. *Journal of Power Sources*, vol. 161, pp. 707-722, 2006.

[14] M. G. Villalva, J. R. Gazoli and E. R. Filho. Comprehensive Approach to Modeling and Simulation of Photovoltaic Arrays," *IEEE Transactions on Power Electronics*, vol. 24, pp 1198 - 1208, 2009.

[15] H. De Battista, H. J. Mantz, F. Garelli. Power Conditioning for a Wind-Hydrogen Energy System. *Journal of Power Sources*, vol. 155, pp. 478-486, 2006.

[16] H. L. Tsai. Insolation-Oriented Model of Photovoltaic Module using Matlab/Simulink. *Solar Energy*, vol. 84, pp. 1318-1326, 2010.

[17] A. S. Al Busaidi, H. A. Kazem, A. H. Al-Badi and M. F. Khan, "A Review of Optimum Sizing of Hybrid PV–Wind Renewable Energy Systems in Oman," *Renewable and Sustainable Energy Reviews*, vol. 53, pp.185-193, 2016.

[18] A. M. Eltamaly, M. A. Mohamed and A. I. Alolah. A Novel Smart Grid Theory for Optimal Sizing of Hybrid Renewable Energy Systems," *Solar Energy*, vol. 124, pp.26-38, 2016.

[19] Z. Shi, R. Wang and Zhang, T. Multi-objective Optimal Design of Hybrid Renewable Energy Systems using Preference-Inspired Coevolutionary Approach," *Solar Energy*, vol. 118, pp.96-106, 2015.

[20] M. S. Ismail, M. Moghavvemi and T. M. I. Mahlia. Genetic Algorithm based Optimization of Modeling and Design of Hybrid Renewable Energy Systems," *Energy Conversion and Management*, vol. 85, pp.120-130, 2014.

[21] H. R., Shakouri, H. G. Amalnick and M. Sadegh, Economic Sizing of a Hybrid (PV-WT-FC) Renewable Energy System (HRES) for Stand-Alone usages by an Optimization-Simulation Model: Case study of Iran," *Renewable and Sustainable Energy Reviews*, vol. 54, pp.139-150, 2016.

[22] E. M. Natsheh, A. Albarbar, and J. Yazdani, Modeling and Control for Smart Grid Integration of Solar/Wind Energy Conversion System. *Innovative Smart Grid Technologies (ISGT Europe), 2011 2nd IEEE PES International Conference and Exhibition*.

[23] K. Ishaque, Z. Salam, H. Taheri, Syafaruddin. Modeling and Simulation of Photovoltaic (PV) system during Partial Shading based on a Two-diode Model. *Simulation Modeling Practice and Theory*, vol. 19, pp. 1613-1626, 2011.

[24] W. De. Soto, S. Klein and W. A. Beckman. Improvement and Validation of a Model for Photovoltaic Array Performance. *Solar Energy*, vol. 80, 78-88, 2006.

[25] A. Shukla, M. Khare, K. N Shukla. Modeling and Simulation of Solar PV Module on MATLAB/Simulink. International Journal of Innovative Research in Science, *Engineering and Technology*. vol. 4, Issue 1, 2015.

[26] M. G. Sobamowo, B.Y. Ogunmola, J. A. Ogbemhe. Analysis of dynamic behavior and power generation of a wind-tidal system for marine environment. *Conference: Proc. ICCEM (2012), January 2012*.

[27] M. G. Sobamowo. Modeling of Power generation in a Hybrid PV-Thermal and Wind Power Systems with an Incorporated Ultracapacitor considering Thermal and Electrical losses. Department of Mechanical Engineering, University of Lagos, Nigeria.